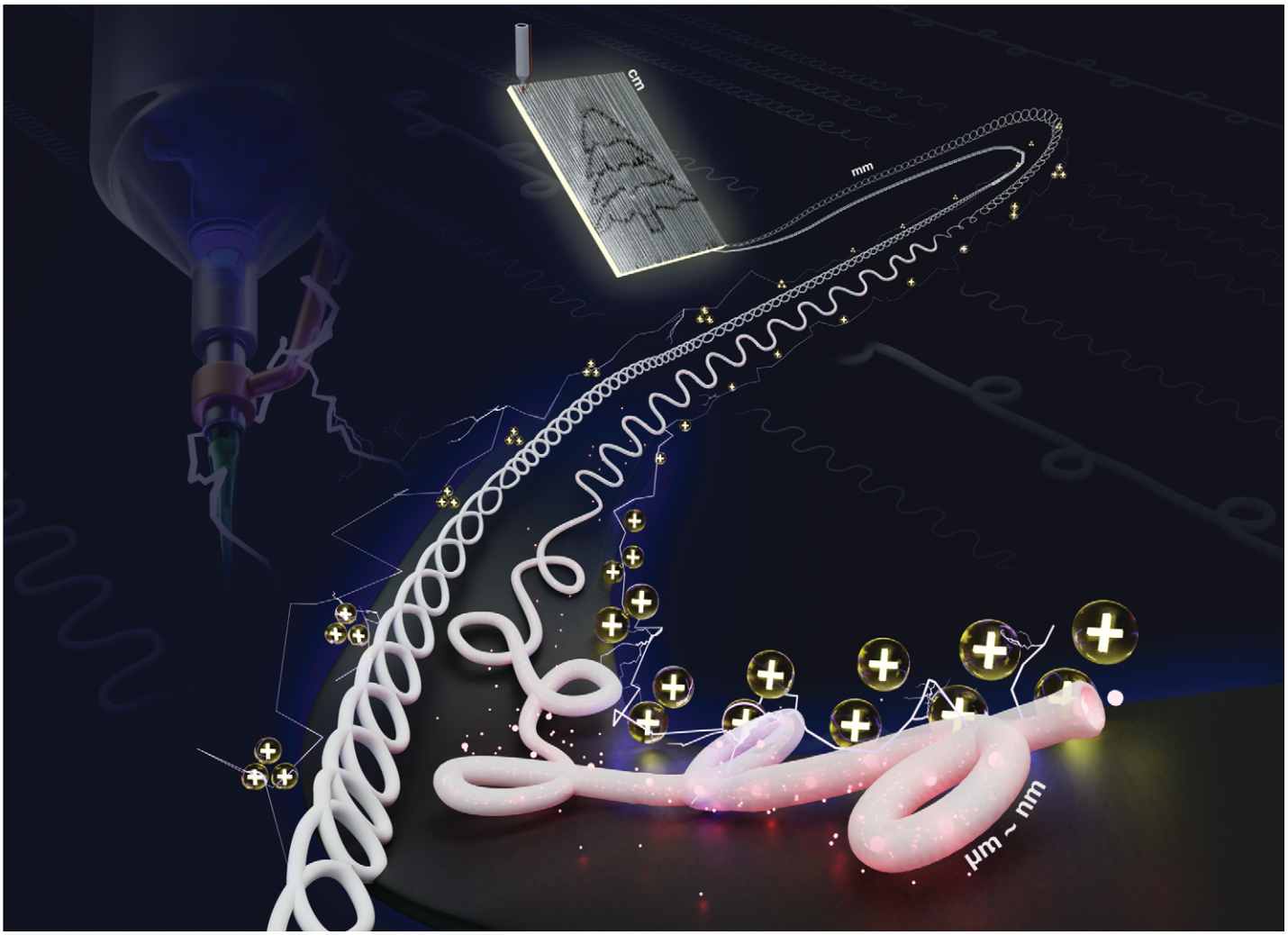

Showcasing research from Dr. Ho Cheung (Anderson) Shum's Microfluidics and Soft Matter Group, Department of Mechanical Engineering, University of Hong Kong, Hong Kong.

Electrocoiling-guided printing of multiscale architectures at single-wavelength resolution

An electrically assisted coiling jet-based technique is introduced to print nanofibers with programmable patterns. Using this approach, we can swiftly switch filament patterns, enhancing the pattern resolution down to the micrometer range. Centimeter-sized architectures constructed from the programmable fiber can be completed in a few minutes.

As featured in:

See Ho Cheung Shum *et al.*, *Lab Chip*, 2019, **19**, 1953.

ROYAL SOCIETY OF CHEMISTRY | Celebrating IYPT 2019

rsc.li/loc

Registered charity number: 207890

Lab on a Chip

PAPER

View Article Online
View Journal | View Issue

Cite this: *Lab Chip*, 2019, **19**, 1953

Electrocoiling-guided printing of multiscale architectures at single-wavelength resolution†

Jingmei Li,‡[ab] Tiantian Kong,‡[c] Jiazuo Yu,[a] Kit Hang Lee,[a] Yuk Heng Tang,[ab] Ka-Wai Kwok,[a] Ji Tae Kim[a] and Ho Cheung Shum *[ab]

Received 13th February 2019,
Accepted 12th April 2019

DOI: 10.1039/c9lc00145j

rsc.li/loc

The rope coiling observed in liquid ink with high viscosity has been exploited in additive printing to fabricate architectures with periodically curled structures and tune their mechanical properties. However, the control over the coiling path relying on mechanical motion restricts the spatiotemporal resolution. We develop an electrically assisted high-resolution technique to manipulate coiling paths of viscous ink and structures of the deposited filament. By spatially programming the voltage applied onto the viscous ink, we show that the switching between different filament structures can be accomplished at single wavelength resolution, facilitating the rapid and accurate construction of sophisticated patterns. Furthermore, translational guiding of the electrocoiling enables rapid printing of filaments with complex structures at a line speed of 10^2 mm s^{-1}. With a simplified trajectory of the printing head, large-area and multiscale patterns can be printed at an unprecedented speed; for instance, centimeter-sized architectures constructed from nanofibers with micron-sized curled structures can be completed in a few minutes. By enabling the printing of complex fiber networks with tunable shape and density, our work provides a route towards custom-design of fiber architectures with unique features such as spatially varying mechanical properties.

Introduction

In Nature, many objects have developed multiscale structures that give rise to materials properties adapted to the natural environment.[1–4] For example, numerous vascular plants contain curled components that enhance their stretchability, efficiency in transporting water and nutrients, and seed dispersal;[5–8] these include lotus roots, tendrils of bitter melon, and leaves of passion fruits and banana.[9] In microorganisms such as bacteria, flagella also possess helical parts that facilitate their locomotion.[6] Inspired by these natural objects, artificial fabrics, actuators and sensors have adopted curled and porous components to give them unique properties.[5,8,10–23] Large networks assembled from curled filaments exhibit properties such as negative Poisson ratios,[24] tunable elasticity and ultra-stretchability,[25] which are different from networks with straight filaments.[26–29] These attributes of networks composed of curled filaments are useful for applications such as strain sensors, filtration membranes and tissue scaffolds.[26,30,31]

When a large network with curly components is needed, direct extrusion-based printing that allows programmable printing paths is preferred as a fabrication approach.[32–34] However, the printing efficiency is reduced with increasing length of the printing paths, which in turn increases with curliness of the networks. To remove the need to match the printing path to the desired network, independent trigger and control of the ink jet to coil have been introduced. Like an elastic rope, a slender viscous jet can bend and rotate steadily, when it falls on a solid substrate.[35–40] When combined with a linearly-translating substrate, the coiling jet has been exploited to print curled filaments as templates into patterns, including meanders, alternating loops and translated coils.[30,41–46] By simplifying the printing paths from curled lines to straight lines, the total length of the moving path is reduced, speeding up the fabrication process. Moreover, the printing speed and accuracy are no longer hampered by acceleration-and-deceleration of the nozzle when making turns. The consequent enhancement in the printing efficiency is particularly significant for networks that consist of filaments with a high degree of curliness.

[a] *Department of Mechanical Engineering, University of Hong Kong, Pokfulam Road, 999077, Hong Kong. E-mail: ashum@hku.hk*
[b] *HKU-Shenzhen Institute of Research and Innovation (HKU-SIRI), Shenzhen, China*
[c] *China Guangdong Key Laboratory for Biomedical Measurements and Ultrasound Imaging, Department of Biomedical Engineering, Shenzhen University, 518037, China*

† Electronic supplementary information (ESI) available: Additional figures: jet velocities as a function of the applied voltage for different polymer concentrations in precursor inks; scanning transmission microscopy images of printed nanofilaments with different curled patterns; comparison of the observed and targeted velocity profiles of the translation platform (PDF). See DOI: 10.1039/c9lc00145j

‡ These authors contributed equally to this work.

Although the rope coiling effect has shown its potential in printing large-scale curled patterns, its wider use is restricted by the challenge to fabricate these patterns with high-resolution in a programmable and controlled manner. In order to control the filament patterns, current approaches still exploit the mechanical movements of the printing platform, for example changing the nozzle-to-substrate distance or the velocity of the moving substrate.[43,44,47–50] These mechanical movements with vibrations and residual motions lead to undesired patterns, especially when the changes in the printing paths are fast and frequent, deteriorating the integrity and functionality of the resultant networks. Moreover, these defects are pronounced for high-resolution fabrication at scales below the micron range. Thus, new methods to improve the precision and quality are still in great demand.

Electro-coiling, by which liquid coiling is assisted by electrically charging the liquid jet, has been recently introduced and studied.[51,52] In this paper, we further develop the electro-coiling method for scalable generation of complex patterns and structures at single-wavelength-resolution. The key idea is to precisely program the coiling by electric pulses at 10 kHz resolution, resulting in instant and seamless switching of curled patterns. We elucidate the effect of the applied voltage on the jet morphology and resultant networks. The gained understanding allows the programmable printing of sophisticated micropatterns from tunable curled nanofibers. As demonstrated in this work, electro-coiling-based printing creates new opportunities to custom-design fiber patterns with multiple structures and tunable diameters. This approach can be extended to print multi-phase fibers, which exhibit great potential to achieve delivery of active ingredients from the patterns.

Experimental section

The printing system consists of an ink delivery system, a high electric field generator and a programmable 3-axis *XYZ* translation stage (Wisequick, China). The precursor ink stored in syringes is delivered using a syringe pump (Cetoni, Germany) at a constant flow rate to an extruding nozzle *via* a segment of micro-tubing (Scientific Commodities Inc. USA). The ink is charged when passing through the nozzle with a high-voltage power amplifier (Trek, USA) coupled with a signal generator (RIGOL Technologies Inc. USA). Below the metallic nozzle, a piece of indium tin oxide (ITO)-coated glass is used as the ground electrode and the substrate to collect the printed filaments. The substrate is placed on a programmable 3-axis *XYZ* translation stage for constraining its movement to desired trajectories. The fastest translation speed we used for the linear translation stage is 200 mm s^{-1}. In our experiments, we also use a rotation stage (magnetic stirrer, IKA, USA) to control the movement of the substrate. The typical moving speed for the rotation stage is in the range of 314–628 mm s^{-1} at about 1 cm away from the center of rotation.

To print the micro-sized filament with a single phase, we use 17–19 wt% polycaprolactone (PCL) (CapaTM 6500, Persorp)-in-chloroform solutions as ink precursors. The nozzle size employed is 500 μm and the nozzle-to-substrate distance is 4 mm. To fabricate the nano-sized filament with a single phase, 10–16 wt% PCL-in-chloroform solution is dispensed from a 30 μm nozzle at a distance of 2 mm from the substrate. The 30 μm nozzle is fabricated from a tapered glass capillary (World Precision Instruments, Inc.) with an inserted metallic wire. To print the core–shell filament, we use 21 wt% PCL-in-chloroform solution as the shell ink and 50 wt% polyethylene glycol (PEG) (Mn = 200, Shanghai Aladdin Bio-Chem Technology, China) containing 1 mg ml^{-1} Rhodamine 6G (Shanghai Aladdin Bio-Chem Technology, China) as the core ink.

To analyse the release rate of the encapsulated ingredients (Rhodamine 6G), we use a microplate reader (SpectraMax id3, Molecular devices, USA) to read the intensity of the fluorescence signal in the solution. The sample is prepared as a fiber network of a size of 4 cm × 4 cm with a thread count of 20 threads per centimetre (TPC), which is constructed with the core–shell filament. During the testing, the sample is separated and transferred to a release medium (3 ml pure water) in a controlled time interval.

To demonstrate the printing of a customized structure of the fiber network, we first map the desired structure into a grayscale picture. For instance, we use white (grayscale = 255) to represent translated coiling filaments that have a length ratio of 6, dark gray (grayscale = 26) to represent meandering filaments that have a length ratio of 1.5, and black (grayscale = 0) to represent straight filaments that have a length ratio of 1. Then, we use a MATLAB code to read the grayscale value in each pixel along the printing trajectory. After acquiring an array of grayscale values, we map it into the electric signal according to the calibrated relationship between the fiber patterns and the applied voltage. The transferred electric signal is then read into a LabVIEW programme, exported through a digital to analog converter and amplified using a high-voltage power amplifier. In this manner, the customized structure can be converted into a grayscale map, which can be subsequently printed.

Results and discussion

Using the electro-coiling method, electrical charging can trigger and manipulate the coiling of viscous jets, as shown in Fig. 1. Without an applied voltage, the viscous ink forms a millimeter-sized meniscus at the nozzle and then flows towards the substrate to form a liquid filament connecting the meniscus and the nozzle, as shown in Fig. 1a. If the substrate is translated, the jet is dragged to form a straight filament or bead-on-a-string pattern on the substrate, depending on the translation velocity V_p, as shown in Fig. 1b.

When the applied voltage is increased to 2.3 kV, the liquid surface is deformed by a sufficiently large electric stress, resulting in a cone-shaped meniscus. The semi-vertical angle of the liquid cone increases from 15° to 25° with increasing voltage from 2.3 kV to 3.0 kV, as shown in Fig. 1a. In the

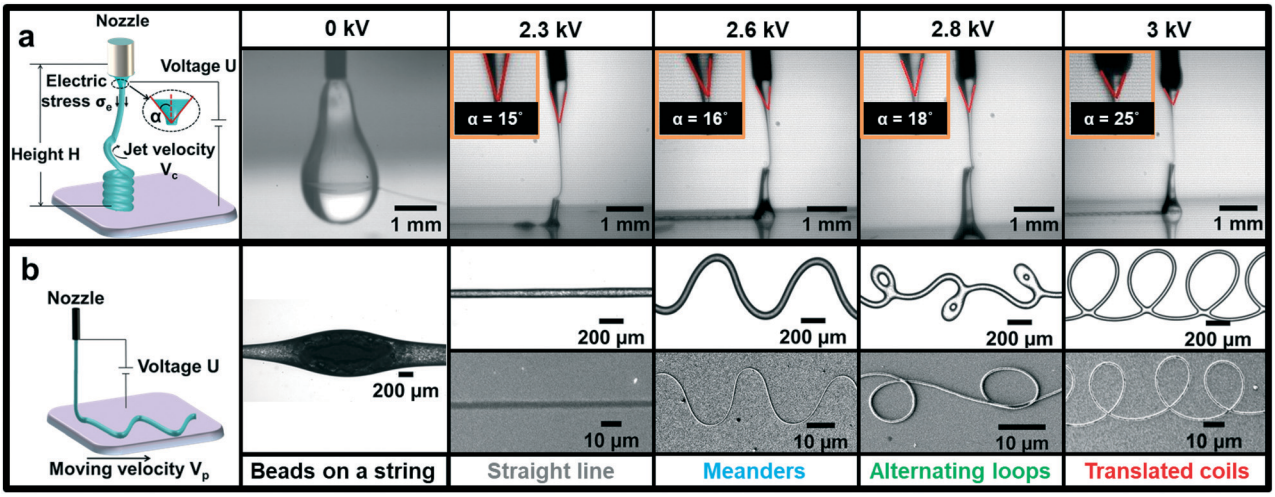

Fig. 1 Electrical coiling of a viscous jet. (a) A viscous liquid jet falls onto a static substrate with an applied voltage of 0 kV, 2.3 kV, 2.6 kV, 2.8 kV & 3.0 kV, respectively; α is the semi-vertical cone angle. (b) A viscous liquid jet falls onto a translated platform with a translation velocity V_p. The liquid jets show various patterns, including beads-on-a-string, straight lines, meanders, alternating loops and translated coils.

electro-coiling regime, the diameter of the liquid jet can decrease ten-fold in comparison with that of the uncharged jet. Due to mass conservation, the velocity of the liquid approaching the substrate must increase significantly from about 1 mm s^{-1} without charging to around 500 mm s^{-1} at an applied voltage of 3 kV. When the liquid jet hits the substrate at such a high velocity, a compressive stress which occurs due to the obstruction of the static substrate forces the liquid jet to coil.[35,41,53] As the applied voltage is further increased, the jet diameter decreases while the coiling frequency increases.

When a coiling jet is dispensed onto a linearly translated substrate, the rotating jet draws periodic filament patterns, as shown in Fig. 1b. Since the coiling frequency and velocity can be tuned by changing the applied voltage, the pattern of the filaments can be varied between straight lines, meandering curves, alternating loops and translated coils conveniently. Upon further increase in the applied voltage, the translated filament will lose its periodicity and become chaotic due to the instability caused by the repulsion between excessive electric charges on the filament surface, as shown in Fig. S1.†[54] The formation of filaments with chaotic patterns is beyond our discussion here.

In addition to the filament patterns, the diameter of the curled filament can be easily tuned by varying the applied voltage. It decreases from around one hundred micrometers to tens of micrometers when the applied voltage increases from 2.1 kV to 3.0 kV. By adjusting the concentration of the polymer in liquid inks as well as the nozzle diameter, the size of the polymer fiber can be further reduced to the nanometer scale in the same range of applied voltage, as shown in the scanning electron microscopy (SEM) images in Fig. 1b and Fig. S2a.† This printing approach is also general and can be applied to not only PCL but also other materials such as poly(lactic acid) (PLA) and poly(lactic-*co*-glycolic acid) (PLGA), as shown in Fig. 2.

To characterize the patterns of the curled filament, we define the length ratio, λ, which is the ratio between the arc length of the filament, S, and the wavelength of the pattern laid on the substrate, L, as shown in Fig. 3a. This length ratio, λ, is approximately equal to the velocity ratio between the coiling jet V_c and the platform V_p, if $V_c > V_p$.[45] Since V_c and V_p are independent (Fig. 3b), and V_c can be effectively tuned by changing the applied voltage (Fig. 3c), the agreement between the measured λ and predicted value by V_c/V_p shows that we can tune λ by adjusting the applied voltage (Fig. 3d). In agreement with previous studies,[45] patterns of straight lines, meanders, alternating loops and translated coils nearly correspond to $\lambda = 1$, $1 < \lambda < 1.8$, $1.7 < \lambda < 3$ and $2.3 < \lambda$, respectively (Fig. 3e). Thus, both the λ and filament shapes can be controlled by varying the applied voltage U and the velocity of the platform V_p.

The fast and seamless switching among the different patterns is key to diversifying the structure of the printed filaments and thus the mechanical properties of the constructed fiber network. Tuning either V_c or V_p can result in pattern switching. To compare the effectiveness of the two approaches, we measure the transitional length of the filament

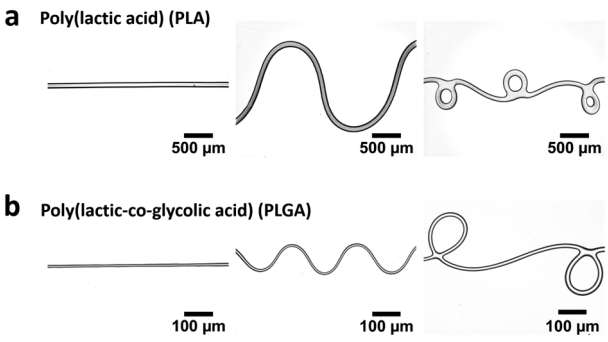

Fig. 2 Optical microscopy image of filaments of (a) poly(lactic acid) (PLA) and (b) poly(lactic-*co*-glycolic acid) (PLGA).

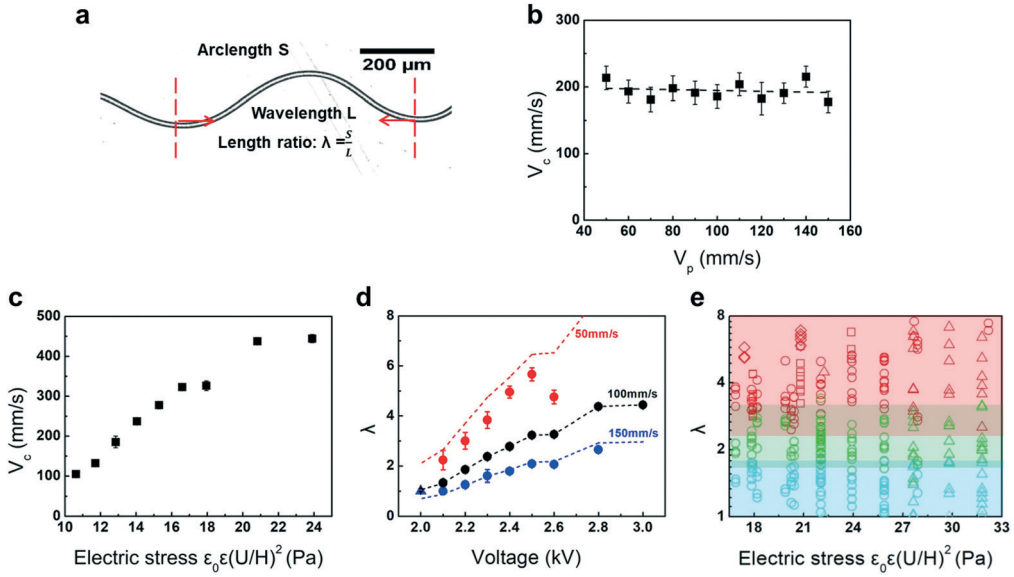

Fig. 3 (a) Optical microscopy image of a printed filament. The length ratio λ is defined as the ratio of arclength S to wavelength L. (b) V_c as a function of the velocity of the platform V_p. The fitted dashed line with a slope of −0.06 indicates that V_c is independent of V_p. (c) Jet velocity as a function of the applied electric stress. V_p = 100 mm s^{-1}. (d) λ as a function of voltage for several V_p values. Each color corresponds to a different V_p value. Red: V_p = 50 mm s^{-1}; black: V_p = 100 mm s^{-1}; blue: V_p = 150 mm s^{-1}. Dots are measured λ, while the dashed lines are the predicted length ratios based on the calibrated V_c from (c). (e) A state diagram of the filament patterns as a function of the length ratio and applied electric stress. Each color corresponds to a different filament pattern. Red: translated coils; green: alternating loops; blue: meanders; grey: straight lines. Each symbol corresponds to a different dielectric constant and flow rate. Square: dielectric constant, ε = 4.8 and flow rate, Q = 1 ml h^{-1}; diamond: ε = 4.8 and Q = 0.5 ml h^{-1}; circle: ε = 6.9 and Q = 1 ml h^{-1}; triangle: ε = 9.1 and Q = 1 ml h^{-1}.

between the patterns before and after complete switching. For the approach of tuning V_p, we fix U = 2.8 kV, and curled filaments with λ = 3 and λ = 1.5 occur at V_p = 100 mm s^{-1} and 200 mm s^{-1}, respectively. It takes about a filament length of 30 mm to complete the transition, for the substrate with a uniform acceleration of around 500 mm s^{-2}. Instead of changing V_c, as we vary U from 2.8 kV to 2.3 kV at V_p = 100 mm s^{-1}, the change in patterns is completed within one cycle of coiling, which has a period of around 7 ms, with a corresponding filament length of 0.7 mm. Experimentally, the transitional filament length and transition time observed can be as low as 20 μm and of 0 (10^{-4} s), respectively (Fig. S2b†). Based on our results, sequential changes in the filament patterns through varying the applied voltage and thus the coiling frequency can be achieved almost seamlessly, as shown in Fig. 3a–c and S2b.† Therefore, tuning the applied voltage is significantly more effective than tuning the velocity of the substrate.

The fast switching between patterns is important for ensuring the accuracy of the printed patterns, especially when frequent switching is needed. To illustrate this, we print a fiber with alternating segments of translated coiling filaments

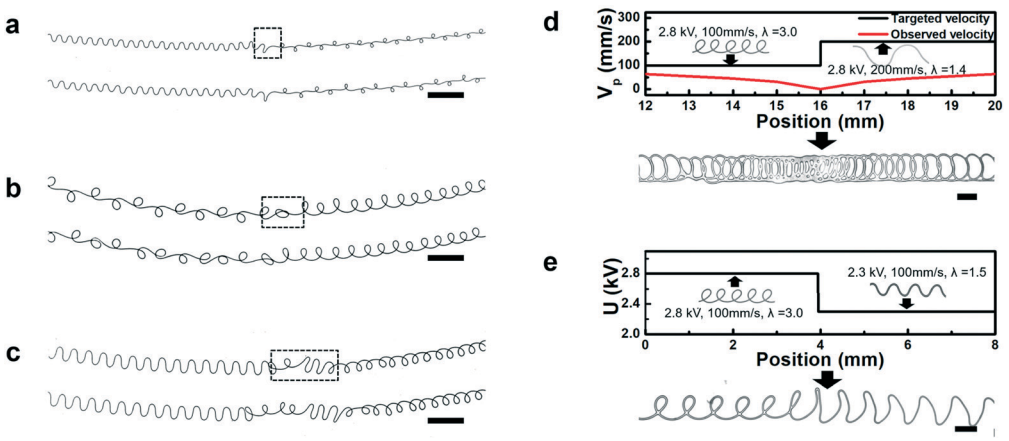

Fig. 4 The switching of the filament patterns. By changing the applied voltage, filament patterns can be switched from (a) meanders to alternating loops, (b) alternating loops to translated coils and (c) meanders to translated coils. Segmented filament printed by (d) tuning the velocity of the platform V_p and (e) changing the applied voltage U. Scale bars are 500 μm.

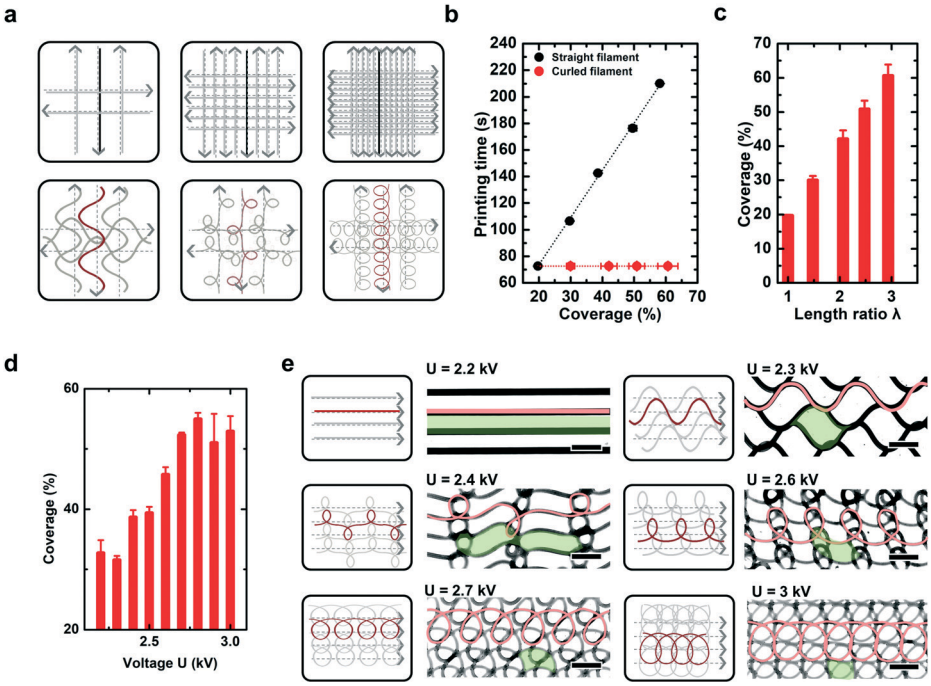

Fig. 5 Fiber networks are printed by depositing fibers line-by-line. (a) Control of the coverage through varying the gap distance between two neighbouring print paths (grey dashed lines) when depositing the straight filament (black lines) or through varying the length ratio of the deposited curled filament (red line). (b) Printing time as a function of the target coverage through depositing the straight filament (black dots) and curled filament (red dots), respectively. V_p = 50 mm s^{-1}. (c) Coverage as a function of the length ratio λ of the constituent filaments. All the filaments have similar diameter, which is around 100 μm. Coverage of the ink (d) and structure of the fiber network (e) changes with the applied voltage U. The fiber networks constructed from curled filaments show periodic repeating units of pores that are marked in green. The constituent filaments are marked in red. Scale bars are 500 μm.

(λ = 3) and meandering filaments (λ = 1.5) by setting V_p = 100 mm s^{-1} and V_p = 200 mm s^{-1}, respectively. Each segment has a length of 8 mm, sequentially. When V_p alternates every 8 mm, the resultant filaments change between translated coiling with λ = 12 and λ = 6, without achieving the meandering shape (Fig. 4d). The significant mismatch between the designed and printed patterns is caused by the difference in the observed and the target platform velocities, as shown in Fig. S3.† In comparison, by applying a square wave of voltage from 2.8 kV to 2.3 kV, the pattern of the resultant filament rapidly switches from translated coiling (λ = 3) to meandering (λ = 2), as shown in Fig. 4e. Therefore, fast switching by varying the applied voltage enhances the accuracy of printing with multiple segments of fiber patterns.

In conventional printing, straight fibers are often woven to form a network. The surface coverage, which is defined as the fraction of covered substrate area after depositing ink materials, is associated with the performance of the architected material, such as permeability. It is essential to evaluate the printing speed when a higher coverage is required. To evaluate the printing speed enhanced by directly extruding the coiling filament, we print networks with coverage values between 20% and 60% by depositing straight and curled filaments, respectively, and then measure the time spent in fabricating a fiber network with a size of 40 mm by 40 mm. Conventionally, using the straight fiber as the constituent filament, the coverage is normally controlled by designing a suitable gap distance between two neighbouring print paths. By contrast, with direct deposition of the curled filament, the coverage can be varied by tuning λ of the coiling filament, as shown in Fig. 5a. While both approaches achieve similar coverage, our experimental results (Fig. 5b) clearly demonstrate that directly using the curled filament as the constituent filament can save time due to the simplification of the print path. As the filament diameters are kept constant, desired coverage can be achieved by controlling λ of the curled filament, since the coverage increases linearly with λ due to mass conservation (Fig. 5c). To spatially vary the local coverage of the ink in different parts of architected materials, λ has to change quickly and precisely. As frequent change in the flow rate of the ink is not applicable, the electro-coiling method offers an approach to vary the coverage through tuning the applied voltage. In the case of applying a constant flow rate, although the fiber width decreases with increasing applied voltage, the measured coverage improves due to the rapid increase in fiber length, as shown in Fig. 5d.

Directly depositing the curled filament enhances the printing speed not only in the case of achieving high coverage but also in the printing of periodic porous structures. Without frequently accelerating and decelerating to adjust the curled print path, porous structures can be printed by directly depositing the curled filament line by line. The structures of the fiber network can be varied by changing the applied voltage, as shown in Fig. 5e.

Enabled by the fast switching of the filament patterns through changing the applied voltage, a well-defined fiber network with spatially heterogeneous structures is achieved. Complex microstructures can be woven by combining segments of filaments with controllable patterns or by splicing various fiber meshes together, as shown in Fig. 6a and b. Furthermore, sophisticated fiber structures with single-wavelength resolution can be conveniently printed using different fiber patterns by applying a translated electric signal to charge the ink, as shown in Fig. 6c. The change in the fiber pattern is achieved merely by adjusting applied voltages, using a single nozzle without changing the ink formulation or flow rate under constant translation velocity. As such, the structure of the printed fiber network follows the spatial distribution of the electric voltages accurately.

To print a customized structure of the fiber network, we can first map the structure into the spatial distribution of the electric signal according to the calibrated relationship between the fiber patterns and applied voltage. Then, based on the moving route of the platform, the electric signal in the time domain can be translated to different filament patterns. Hence, using this electro-coiling printing approach, the network structures can be programmed *via* the profile of the applied voltage, similar to that in a regular printer.

Besides a single-phase fiber pattern, the method can be extended to print multi-phase fibers through modification of the nozzle. For instance, using a coaxial needle, we can encapsulate aqueous droplets inside a shell material for encapsulation of aqueous active ingredients. To demonstrate this, we encapsulate a model fluorescent active ingredient, Rhodamine 6G, within our patterned fibers, whose morphology can be manipulated by tuning the flow rates of the fluorescent inner phase. At high flow rates, core–shell fibers with a continuous thread of the inner phase are fabricated, as shown in Fig. 7a, while fibers with droplets of the inner phase are formed at low flow rates, as shown in Fig. 7b.

The release process of the dye is shown in Fig. 7c. The relative fluorescence intensity is measured every 1 minute, right after separating and transferring our core–shell fiber from one tube with 3 ml water into another.

Conclusions

The ability to design and rapidly fabricate materials with complex and accurate patterns is crucial for diversifying the function of the created architectures. In this work, we demonstrate an electrically assisted technique for fabricating complicated microstructures at single-wavelength resolution

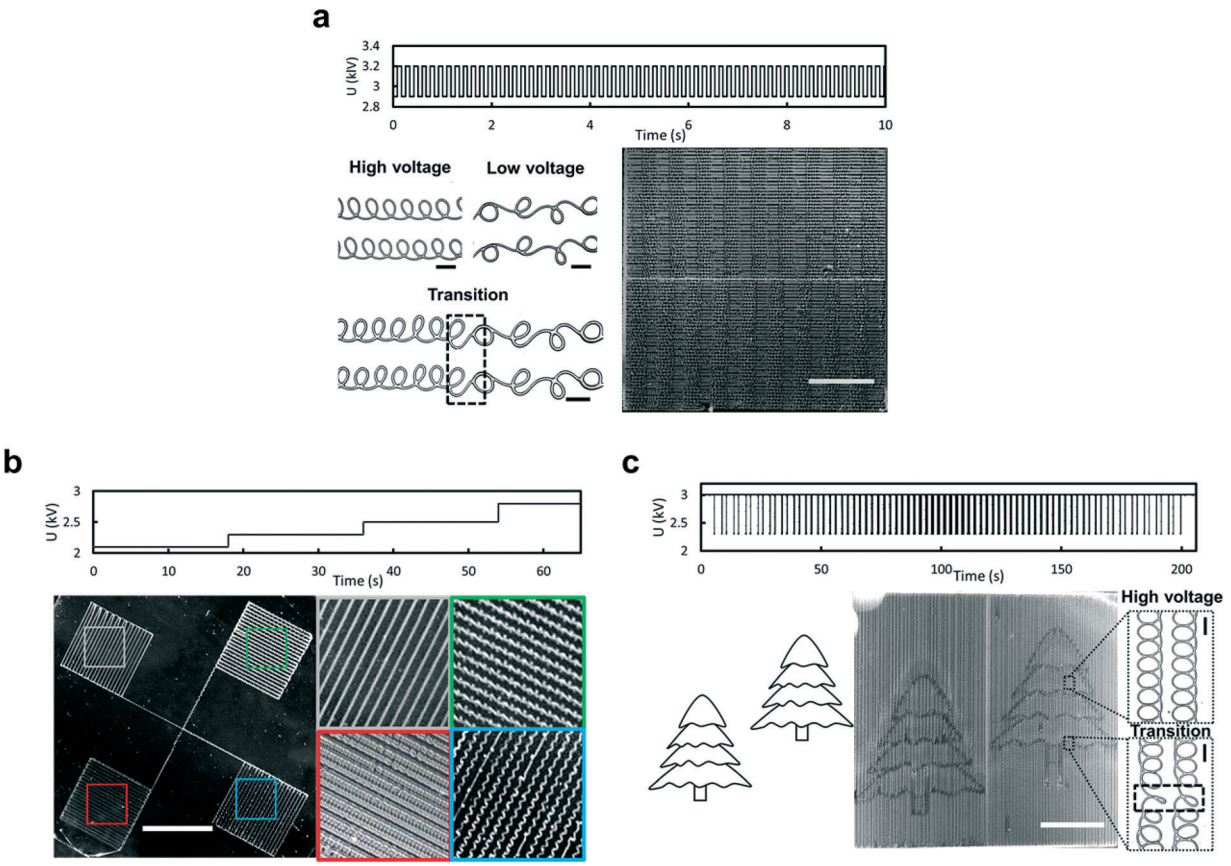

Fig. 6 The structures of the fiber network are designed by programming voltages along the printing paths. (a) Square waves are applied to vary the filament patterns between alternating loops and translated coils. (b) Slices of four different structures are printed by a stair-up wave (3 stairs). (c) Pictures of a tree are printed by applying the corresponding transformed electric signal to outline the objects by different filament patterns. Black scale bars are 500 μm. White scale bars are 20 mm.

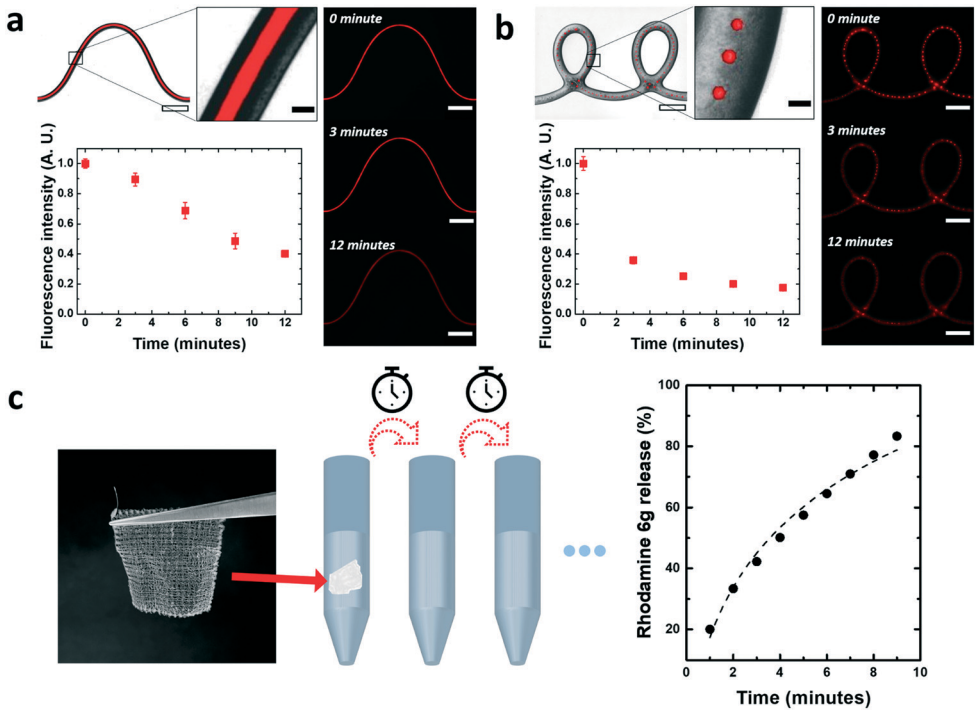

Fig. 7 Release of an aqueous dye from core–shell fibers printed using our technique. Inside the core–shell fiber, the core liquid phase of a polyethylene glycol (PEG) solution contains a fluorescent dye. (a) Fluorescence microscopy images of the compound jet formed at a core phase flow rate of 400 μl h^{-1} and the corresponding release profile of the dye; (b) fluorescence microscopy images of a core–shell fiber with the dye solution encapsulated in the form of droplets at a core phase flow rate of 100 μl h^{-1} and the corresponding release profile of the dye. White scale bars are 500 μm, and black scale bars are 100 μm. (c) Photograph of a 4 cm × 4 cm fiber network consisting of core–shell fibers with dye solution encapsulated and the corresponding release profile. To test the release of the dye, the fiber network is transferred to a new tube with 3 ml water every 1 minute.

from a coiling inkjet. Different filament structures, including straight lines, meanders, alternating loops and translated coils, can be controllably fabricated by manipulating the applied voltage onto the inkjet. Using the electro-coiling method, the switching in filament patterns is significantly accelerated. The transitional length of the filament can be reduced to micrometers. The fast and seamless switching between different curled nanofibers using one nozzle enables rapid and accurate construction of sophisticated fiber networks. Furthermore, our techniques can be conveniently adopted for printing single-phase and multiple-phase compliant fiber patterns, which are promising for encapsulating and releasing active ingredients. Hence, our work provides a route towards custom-design of fiber architectures with spatially addressable mechanical properties.

Conflicts of interest

The authors declare that there is no conflict of interest in the materials submitted in this manuscript.

Acknowledgements

We thank Prof. N. Ribe (Laboratoire FAST - Bat. 502 Campus Universitaire, France) for the critical comments on and modifications in the manuscript. This research was supported by the General Research Fund (HKU 719813, 17304514 and 17306315, 17202317) from the Research Grants Council of Hong Kong.

Notes and references

1 H. Chen, P. Zhang, L. Zhang, H. Liu, Y. Jiang, D. Zhang, Z. Han and L. Jiang, *Nature*, 2016, **532**, 85–89.
2 Y. Forterre and J. Dumais, *Science*, 2011, **333**, 1715–1716.
3 U. G. K. Wegst, H. Bai, E. Saiz, A. P. Tomsia and R. O. Ritchie, *Nat. Mater.*, 2014, **14**, 23–26.
4 W.-G. Kim, H. Song, C. Kim, J.-S. Moon, K. Kim, S.-W. Lee and J.-W. Oh, *Biosens. Bioelectron.*, 2016, **85**, 853–859.
5 S. E. Naleway, M. M. Porter, J. McKittrick and M. A. Meyers, *Adv. Mater.*, 2015, **27**, 5455–5476.
6 X. Yan, Q. Zhou, J. Yu, T. Xu, Y. Deng, T. Tang, Q. Feng, L. Bian, Y. Zhang, A. Ferreira and L. Zhang, *Adv. Funct. Mater.*, 2015, **25**, 5333–5342.
7 P. Xu, R. Xie, Y. Liu, G. Luo, M. Ding and Q. Liang, *Adv. Mater.*, 2017, **29**, 1701664.
8 Y. Yu, F. Fu, L. Shang, Y. Cheng, Z. Gu and Y. Zhao, *Adv. Mater.*, 2017, **29**, 1605765.
9 W. Gao, X. Feng, A. Pei, C. R. Kane, R. Tam, C. Hennessy and J. Wang, *Nano Lett.*, 2014, **14**, 305–310.
10 S. Xu, Z. Yan, K.-I. Jang, W. Huang, H. Fu, J. Kim, Z. Wei, M. Flavin, J. McCracken, R. Wang, A. Badea, Y. Liu, D. Xiao, G. Zhou, J. Lee, H. U. Chung, H. Cheng, W. Ren, A. Banks, X.

Li, U. Paik, R. G. Nuzzo, Y. Huang, Y. Zhang and J. A. Rogers, *Science*, 2015, **347**, 154–159.
11 M. Wu, H. Shuai, Q. Cheng and L. Jiang, *Angew. Chem., Int. Ed.*, 2014, **53**, 3358–3361.
12 J. Li, S. Sattayasamitsathit, R. Dong, W. Gao, R. Tam, X. Feng, S. Ai and J. Wang, *Nanoscale*, 2014, **6**, 9415–9420.
13 K.-I. Jang, H. U. Chung, S. Xu, C. H. Lee, H. Luan, J. Jeong, H. Cheng, G.-T. Kim, S. Y. Han, J. W. Lee, J. Kim, M. Cho, F. Miao, Y. Yang, H. N. Jung, M. Flavin, H. Liu, G. W. Kong, K. J. Yu, S. I. Rhee, J. Chung, B. Kim, J. W. Kwak, M. H. Yun, J. Y. Kim, Y. M. Song, U. Paik, Y. Zhang, Y. Huang and J. A. Rogers, *Nat. Commun.*, 2015, **6**, 6566.
14 S. Xu, Y. Zhang, J. Cho, J. Lee, X. Huang, L. Jia, J. A. Fan, Y. Su, J. Su, H. Zhang, H. Cheng, B. Lu, C. Yu, C. Chuang, T.-i. Kim, T. Song, K. Shigeta, S. Kang, C. Dagdeviren, I. Petrov, P. V. Braun, Y. Huang, U. Paik and J. A. Rogers, *Nat. Commun.*, 2013, **4**, 1543.
15 Y. Yu, L. Shang, W. Gao, Z. Zhao, H. Wang and Y. Zhao, *Angew. Chem.*, 2017, **129**, 12295–12299.
16 W. Wang, X.-H. He, M.-J. Zhang, M.-J. Tang, R. Xie, X.-J. Ju, Z. Liu and L.-Y. Chu, *Macromol. Rapid Commun.*, 2017, **38**, 1700429.
17 L. Liu, L. Zhang, S. M. Kim and S. Park, *Nanoscale*, 2014, **6**, 9355–9365.
18 A. Zhu and M. Guo, *Macromol. Rapid Commun.*, 2016, **37**, 426–432.
19 P. Chen, Y. Xu, S. He, X. Sun, S. Pan, J. Deng, D. Chen and H. Peng, *Nat. Nanotechnol.*, 2015, **10**, 1077.
20 R. Guo, Y. Yu, J. Zeng, X. Liu, X. Zhou, L. Niu, T. Gao, K. Li, Y. Yang, F. Zhou and Z. Zheng, *Adv. Sci.*, 2015, **2**, 1400021.
21 C. B. Cooper, K. Arutselvan, Y. Liu, D. Armstrong, Y. Lin, M. R. Khan, J. Genzer and M. D. Dickey, *Adv. Funct. Mater.*, 2017, **27**, 1605630.
22 J. Park, H. Park, P. Ercius, A. F. Pegoraro, C. Xu, J. W. Kim, S. H. Han and D. A. Weitz, *Nano Lett.*, 2015, **15**, 4737–4744.
23 H. Ceylan, J. Giltinan, K. Kozielski and M. Sitti, *Lab Chip*, 2017, **17**, 1705–1724.
24 A. Clausen, F. Wang, J. S. Jensen, O. Sigmund and J. A. Lewis, *Adv. Mater.*, 2015, **27**, 5523–5527.
25 R. Rahimi, W. Yu, M. Ochoa and B. Ziaie, *Lab Chip*, 2017, **17**, 1585–1593.
26 B. Sun, Y.-Z. Long, S.-L. Liu, Y.-Y. Huang, J. Ma, H.-D. Zhang, G. Shen and S. Xu, *Nanoscale*, 2013, **5**, 7041–7045.
27 Y. Zhang, S. Wang, X. Li, J. A. Fan, S. Xu, Y. M. Song, K.-J. Choi, W.-H. Yeo, W. Lee, S. N. Nazaar, B. Lu, L. Yin, K.-C. Hwang, J. A. Rogers and Y. Huang, *Adv. Funct. Mater.*, 2014, **24**, 2028–2037.
28 M. Su, F. Li, S. Chen, Z. Huang, M. Qin, W. Li, X. Zhang and Y. Song, *Adv. Mater.*, 2016, **28**, 1369–1374.
29 J. K. Nunes, H. Constantin and H. A. Stone, *Soft Matter*, 2013, **9**, 4227–4235.
30 J. Klein, M. Stern, G. Franchin, M. Kayser, C. Inamura, S. Dave, J. C. Weaver, P. Houk, P. Colombo and M. Yang, *3D Print. Addit. Manuf.*, 2015, **2**, 92–105.
31 N. Abdul Rahman, A. R. Gulur Srinivas and J. Travas-Sejdic, *Synth. Met.*, 2014, **191**, 151–160.
32 A. R. Studart, *Chem. Soc. Rev.*, 2016, **45**, 359–376.
33 N. Zhou, C. Liu, J. A. Lewis and D. Ham, *Adv. Mater.*, 2017, **29**, 1605198.
34 E. Cesewski, A. P. Haring, Y. Tong, M. Singh, R. Thakur, S. Laheri, K. A. Read, M. D. Powell, K. J. Oestreich and B. N. Johnson, *Lab Chip*, 2018, **18**, 2087–2098.
35 M. Maleki, M. Habibi, R. Golestanian, N. Ribe and D. Bonn, *Phys. Rev. Lett.*, 2004, **93**, 214502.
36 H.-Y. Kim, M. Lee, K. J. Park, S. Kim and L. Mahadevan, *Nano Lett.*, 2010, **10**, 2138–2140.
37 N. Ribe, H. Huppert, M. Hallworth, M. Habibi and D. Bonn, *J. Fluid Mech.*, 2006, **555**, 275–297.
38 M. Habibi, Y. Rahmani, D. Bonn and N. Ribe, *Phys. Rev. Lett.*, 2010, **104**, 074301.
39 M. Le Merrer, D. Quéré and C. Clanet, *Phys. Rev. Lett.*, 2012, **109**, 064502.
40 N. M. Ribe, M. Habibi and D. Bonn, *Phys. Fluids*, 2006, **18**, 084102.
41 S. Chiu-Webster and J. R. Lister, *J. Fluid Mech.*, 2006, **569**, 89–111.
42 J. Klein, M. Stern, G. Franchin, M. Kayser, C. Inamura, S. Dave, J. C. Weaver, P. Houk, P. Colombo, M. Yang and N. Oxman, *3D Print. Addit. Manuf.*, 2015, **2**, 92–105.
43 T. Han, D. H. Reneker and A. L. Yarin, *Polymer*, 2007, **48**, 6064–6076.
44 R. Passieux, L. Guthrie, S. H. Rad, M. Lévesque, D. Therriault and F. P. Gosselin, *Adv. Mater.*, 2015, **27**, 3676–3680.
45 P.-T. Brun, B. Audoly, N. M. Ribe, T. S. Eaves and J. R. Lister, *Phys. Rev. Lett.*, 2015, **114**, 174501.
46 Y. Hyunwoo and Z. Xuanhe, *Adv. Mater.*, 2018, **30**, 1704028.
47 Y. Xin and D. H. Reneker, *Polymer*, 2012, **53**, 4254–4261.
48 Y. Huang, Y. Duan, Y. Ding, N. Bu, Y. Pan, N. Lu and Z. Yin, *Sci. Rep.*, 2014, **4**, 5949.
49 S. An, C. Stambaugh, S. Kwon, K. Lee, B. Kim, Q. Kim and W. Jhe, *SPIE NanoScience + Engineering*, 2013, vol. 8816, p. 6.
50 A. W. Knoll, M. Zientek, L. L. Cheong, C. Rawlings, P. Paul, F. Holzner, J. L. Hedrick, D. J. Coady, R. Allen and U. Dürig, *SPIE Adv. Lithographic Technologies VI*, 2014, vol. 9049, p. 8.
51 T. Kong, J. Li, Z. Liu, Z. Zhou, P. H. Y. Ng, L. Wang and H. C. Shum, *Sci. Rep.*, 2016, **6**, 19606.
52 T. Kong, H. A. Stone, L. Wang and H. C. Shum, *Proc. Natl. Acad. Sci. U. S. A.*, 2018, **115**, 6159–6164.
53 N. M. Ribe, M. Habibi and D. Bonn, *Annu. Rev. Fluid Mech.*, 2012, **44**, 249–266.
54 M. M. Hohman, M. Shin, G. Rutledge and M. P. Brenner, *Phys. Fluids*, 2001, **13**, 2201–2220.

